



# LUND UNIVERSITY

## The predissociation of highly excited states in acetylene by time-resolved photoelectron spectroscopy

Zamith, S; Blanchet, V; Girard, B; Andersson, J; Ristinmaa Sörensen, Stacey; Hjelte, I; Bjorneholm, O; Gauyacq, D; Norin, Johan; Mauritsson, Johan; L'Huillier, Anne

*Published in:*  
Journal of Chemical Physics

*DOI:*  
[10.1063/1.1589479](https://doi.org/10.1063/1.1589479)

2003

[Link to publication](#)

### *Citation for published version (APA):*

Zamith, S., Blanchet, V., Girard, B., Andersson, J., Ristinmaa Sörensen, S., Hjelte, I., Bjorneholm, O., Gauyacq, D., Norin, J., Mauritsson, J., & L'Huillier, A. (2003). The predissociation of highly excited states in acetylene by time-resolved photoelectron spectroscopy. *Journal of Chemical Physics*, 119(7), 3763-3773.  
<https://doi.org/10.1063/1.1589479>

*Total number of authors:*  
11

### **General rights**

Unless other specific re-use rights are stated the following general rights apply:  
Copyright and moral rights for the publications made accessible in the public portal are retained by the authors and/or other copyright owners and it is a condition of accessing publications that users recognise and abide by the legal requirements associated with these rights.

- Users may download and print one copy of any publication from the public portal for the purpose of private study or research.
- You may not further distribute the material or use it for any profit-making activity or commercial gain
- You may freely distribute the URL identifying the publication in the public portal

Read more about Creative commons licenses: <https://creativecommons.org/licenses/>

### **Take down policy**

If you believe that this document breaches copyright please contact us providing details, and we will remove access to the work immediately and investigate your claim.

LUND UNIVERSITY

PO Box 117  
221 00 Lund  
+46 46-222 00 00

# The predissociation of highly excited states in acetylene by time-resolved photoelectron spectroscopy

S. Zamith, V. Blanchet,<sup>a)</sup> and B. Girard

*Laboratoire de Collisions, Agrégats et Réactivité, IRSAMC-UPS-CNRS, Toulouse, France*

J. Andersson and S. L. Sorensen

*Department of Synchrotron Radiation Research, University of Lund, Lund, S-221 00, Sweden*

I. Hjelte and O. Björneholm

*Department of Physics, Uppsala University, S-75021 Uppsala, Sweden*

D. Gauyacq

*Laboratoire de Photophysique Moléculaire, CNRS, Orsay, France*

J. Norin, J. Mauritsson, and A. L'Huillier

*Department of Physics, Lund Institute of Technology, Lund, S-221 00, Sweden*

(Received 20 December 2002; accepted 14 May 2003)

We study the dynamics of highly excited states in acetylene initiated by an ultrashort vacuum ultraviolet laser pulse. Electronic states lying in the  $4s$ - $3d$  Rydberg region are excited with one femtosecond pulse, and the dynamic development of the states is monitored by a second short pulse which ionizes the system. We show that even for femtosecond pulses where the bandwidth of the exciting pulse covers several electronic states, it is possible to extract short decay lifetimes through time-resolved photoelectron spectroscopy by using a frequency-modulated (chirped) excitation pulse. We report decay lifetimes for the  $F 4_0^2$  and  $E 4-5_0^2$  states in acetylene, and for the  $E 4_0^2$  and  $E 5_0^2$  states in d-acetylene. The time evolution measured in the electron spectra is compared to decay spectra measured using ion yield and the differences in these results are discussed. © 2003 American Institute of Physics. [DOI: 10.1063/1.1589479]

## I. INTRODUCTION

The formation mechanism of amino acids and polyols in the extraterrestrial atmosphere is an important question in biology, planetary astrophysics, and cosmology. The existence of a variety of important species can be traced to interstellar photochemistry taking place in interstellar molecular clouds.<sup>1</sup> Molecular building blocks consisting of simple carbon and nitrogen-based compounds form the basis for complex organic molecules which play a key role in terrestrial biology. Ultraviolet photolysis of these simple molecules is a fundamental mechanism for this process and understanding the steps leading to larger carbon-based systems is a challenge for interstellar chemistry. The most abundant molecules in the interstellar medium include  $H_2$ , CO, and acetylene. A detailed understanding of photoinduced reactions, including direct dissociation and predissociative mechanisms, is implicit to completing the photoreactive scenario behind the formation of larger molecules such as sugars and amino acids. In this work we focus on the dissociation induced by photoabsorption in the ultraviolet region of acetylene and its deuterated isotope. There are very strong absorption bands in the 9–12 eV region of these molecules; the bands consist of overlapping Rydberg series and valence

electronic states. The lifetimes of these states range from picoseconds to a few femtoseconds, even for states lying very close in energy.<sup>2,3</sup>

In the present experiment, we apply a time-resolved spectroscopic technique capable of monitoring dynamics on a femtosecond time scale to Rydberg and valence states in  $C_2H_2$  and  $C_2D_2$  using an ultrashort pump pulse at about 9.4 eV. These states lie in the Rydberg ( $3d$ - $4s$ ) complex at about 2 eV below the ionization threshold. The  $F 1^1\Sigma_u^+(3d\pi_g)$  Rydberg state shows the strongest photoabsorption in this region.<sup>4</sup> All of the Rydberg transitions exhibit vibrational bands corresponding to excitation of the symmetric stretching mode  $\nu_2$  since the C–C triple bond is lengthened compared to the ground state. A weak excitation of the *trans* bending mode  $\nu_4$  is apparent in the  $F$ - $X$  excitation,<sup>5</sup> arising from interaction with the nonlinear  $E$  valence state. These bands have been explored via photofragment action spectroscopy where lifetimes ranging from 60 up to 150 fs were reported.<sup>3,6</sup> Here, we investigate the dynamics from the  $F 4_0^2$  state and the  $E 4-5_0^2$  state. The excitation scheme is shown in Fig. 1: the dissociation dynamics are probed by a transition on to the ionic continuum by a probe pulse.<sup>7,8</sup> The dynamics of the excited state are analyzed through time-resolved photoelectron spectroscopy (PES) and ion spectrometry.<sup>9</sup> There are only two dissociation channels open at the 9.4 eV pump energy.<sup>10</sup> Both lead to  $C_2H$  radical formation (in the  $A 2^1\Pi$  electronic state or the  $X 2^1\Sigma^+$  ground state—with 3600  $cm^{-1}$  energy of separation between the electronic origins<sup>11</sup>). The

<sup>a)</sup>Author to whom correspondence should be addressed. Electronic mail: val@irsamc.ups-tlse.fr

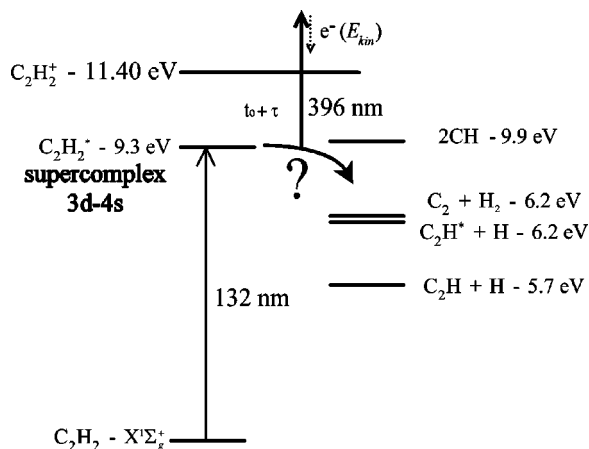


FIG. 1. Principle of the pump-probe experiment.

CH+CH and  $C_2+H_2$  channels are not open at 9.4 eV because the dissociation threshold is at a higher energy for the latter channel, while the former channel is accompanied by a high energy barrier.<sup>12,13</sup>

The density of states is generally high in molecules where close-lying electronic states have overlapping vibrational progressions. Complete selectivity in the excitation of a vibrational sublevel requires narrow bandwidth pulses. These stringent requirements are not always compatible with short pulse durations needed to time-resolve the dissociation dynamics. We illustrate the situation for the case in hand in Fig. 2. The absorption spectra for acetylene and d-acetylene in the region of current interest are shown in the upper panels together with a Gaussian distribution of a pulse energy corresponding to two pump wavelengths, namely  $\lambda_1 = 132.2$  nm ( $75\,643$   $\text{cm}^{-1}$ ) and  $\lambda_2 = 132.0$  nm ( $75\,757$   $\text{cm}^{-1}$ ). Note that in acetylene the  $\lambda_1$  pulse mainly excites the  $F\,4_0^2$  state, while the  $\lambda_2$  pulse excites the  $F\,4_0^2$  state as well as the quasi-degenerate  $E\,4-5_0^2$  states. We use a frequency modu-

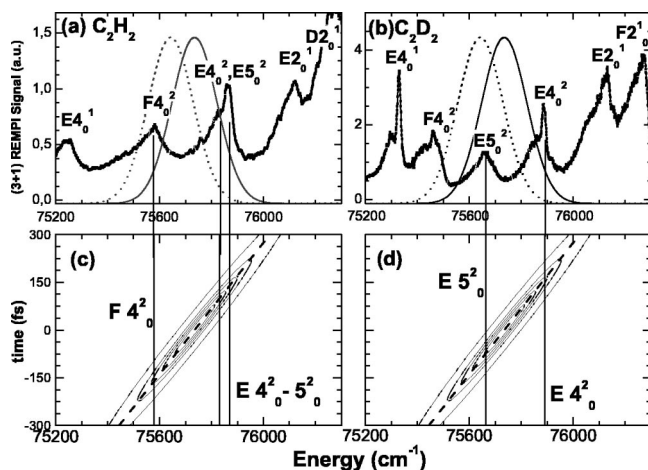


FIG. 2. REMPI (3+1) spectra of (a)  $C_2H_2$  and (b)  $C_2D_2$  together with the pump spectra corresponding to the two different excitation wavelengths (dotted line  $\lambda_1 = 132.2$  nm, solid line  $\lambda_2 = 132.0$  nm). The Wigner representation of the pulse centered at 132.0 nm is plotted in (c) and (d). A positive linear chirp of  $\phi'' = +5330$   $\text{fs}^2$  stretches the pump pulse from 50 to 300 fs FWHM. For both contour plots, the instantaneous frequency of the pump field,  $\omega_p(t)$ , is indicated by the dashed line.

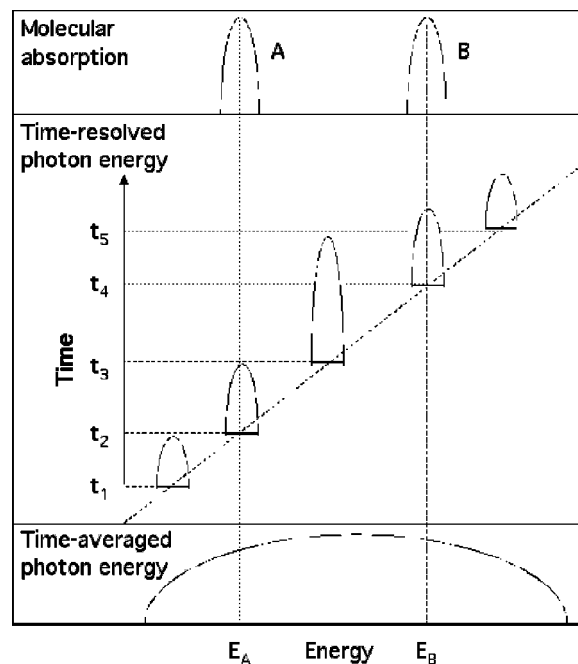


FIG. 3. Principle of time-energy benchmark.

lated (chirped) pump pulse. The Wigner diagram of such a pulse (at the central frequency  $\lambda_2$ ) is shown as a contour plot in the lower panels of Fig. 2: the time axis shows the duration of the pulse, and the dashed slope represents the instantaneous frequency of the pump field. The two states (indicated by the vertical lines in the figure) will be excited at different times as the pulse “sweeps” through the frequency range.

Each excited state will decay on an individual time scale. The interplay between the pump pulse and the molecular electronic states, analyzed by recording the pump-probe signal gives a fingerprint of the system. The molecule provides a *time-energy benchmark*: the energies and lifetimes of the excited states. If the photoelectron bands overlap in the resulting spectra, and if geometry changes occur during the photoionization, it is generally impossible to disentangle the time evolution of each excited state separately, even using energy-dispersive spectroscopy. To circumvent this problem, the pump pulse is frequency modulated (chirped) so that the moment when the frequency is resonant with the state, “time zero,” is different for each excited state. The linear sweep of the pump frequency provides a *time-energy scale*, which can be adjusted to match the *time-energy benchmark* of the molecule.

The concept of *time-energy scale* presented here deserves a thorough explanation. Consider a molecule which can be excited into states A and B by absorption of photons of the two different energies  $E_A$  and  $E_B$ , as indicated in the upper panel of Fig. 3. In our experiment the overall, time-averaged photon energy distribution in the excitation pulse is considerably broader than the energy separation between states A and B, see the lower panel of Fig. 3. Both states A and B will thus be excited by the same pulse. In a time-resolved view, however, the photon energy distribution at any given time  $t_x$  is narrower due to the chirp. As schemati-

cally shown in the middle panel, the “chirp” of the pulse can be described as a sweeping of the photon energy through the envelope of the time-averaged photon energy distribution. Excitation occurs when the photon energy matches the excitation energy and over a time corresponding to the absorption band. The *A* state will be excited at  $t_2$  and the *B* state will be excited at  $t_4$ . The “chirp” can thus be said to provide a *time-energy scale*, as states *A* and *B* are excited at different times. Any dynamic development of states *A* and *B* will thus be separated by this difference in starting time, greatly facilitating the analysis of the spectra. This makes it possible to extract the time-dependent signature for each state from the time-resolved PES. Deuterated acetylene provides a slightly different *time-energy benchmark*, with another response to the chirped pump pulse because of the longer decay times upon deuteration.

Another challenge of this experiment is the use of a femtosecond pump pulse in the vacuum ultraviolet (VUV). A number of techniques are now becoming available to produce short-pulsed, VUV radiation. Most of these techniques use nonlinear processes in a gas.<sup>14</sup> Recent time-resolved dynamic studies have been performed in the VUV and even XUV range<sup>15</sup> using cascade nonlinear wave mixing in a hollow fiber filled with a rare gas,<sup>16</sup> two-photon resonant difference-frequency mixing,<sup>17</sup> and high-order harmonic generation.<sup>18</sup> Refinement of the harmonic-generation technique has led to greater control over the pulse shape<sup>19</sup> and improvement of the pulse-generation efficiency in the VUV-XUV wavelength range shows great promise, in particular for the study of femtosecond dynamics in polyatomic molecules. In the present article, we use the third harmonic of an intense frequency-doubled titanium-sapphire laser as a pump pulse while the probe is taken from the frequency-doubled light.

The experimental setup is described in Sec. II. In Sec. III, we present the time-resolved PES for the two excitation wavelengths used and we compare our results to (3+1) resonant enhanced multiphoton ionization PES (REMPI-PES) using nanosecond laser pulses.<sup>5</sup> The analysis of the photoelectron spectra and the time-dependent ion-yield spectra including the resulting dissociation lifetimes of the excited states is presented in Sec. IV.

## II. EXPERIMENTAL SETUP

The general experimental setup is depicted in Fig. 4. We use the 10 Hz terawatt laser at the Lund high-power laser facility to generate infrared pulses with 100 mJ energy, 110 fs duration, 792 nm central wavelength, and about 10 nm bandwidth. The 396 nm pulse used to generate high-order harmonics and the time-delayed 396 nm probe pulse are generated through frequency doubling in 1.5-mm-thick KDP crystals in a modified Michelson interferometer (see Fig. 4). The pulsed infrared beam is divided into two beams (66% for the pump generation and 33% for the probe) by a beam splitter. A negative lens is inserted in one of the beam paths to focus the two pulses at different distances. A 1.5-mm-thick KDP crystal frequency doubles one of the pulses before they are recombined by a dichroic mirror, which transmits the infrared radiation and reflects the blue (396 nm) light. An

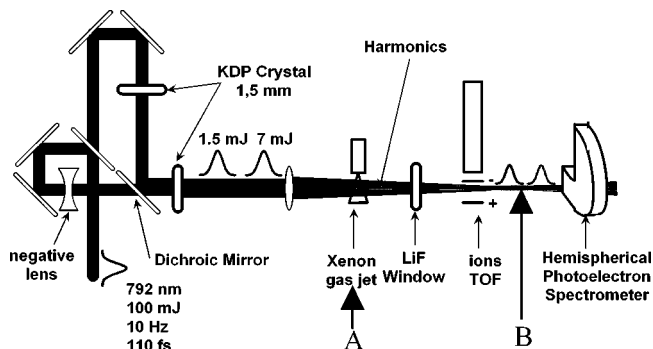


FIG. 4. Experimental setup.

identical KDP crystal doubles the other pulse, and finally the remaining infrared light is filtered away by a second dichroic mirror (not shown). A computer controlled translation stage with 1  $\mu\text{m}$  resolution controls the position of the end mirrors in one of the interferometer arms. This setup allows us to produce pairs of 396 nm pulses, and to control the delay between them. The output energies are 7 mJ for the pulse generating the harmonics and 1.5 mJ for the probe over a 3 cm diameter. A positive lens with a 2 m focal length is then used to focus the two beams. The first beam is focused under the nozzle of a xenon gas jet (point A in Fig. 4) to generate harmonics and the second (probe) beam is focused about 1.3 m from the jet (point B in Fig. 4). The time-resolved experiments utilize the third harmonic (132 nm) as a pump pulse and a probe 396 nm pulse. The fifth harmonic (15.8 eV) by ionizing both the acetylene sample, and the rare gases, allows us to calibrate the photoelectron spectrometer energy scale and resolution, as well as to optimize and align the experimental setup. In the pump/probe experiments, this harmonic is eliminated by using a 3-mm-thick lithium-fluoride (LiF) window after the gas jet. LiF absorbs radiation below 105 nm (11.8 eV). The efficiency for third-harmonic generation in xenon gas is about  $10^{-6}$ , leading to a pulse energy of about 10 nJ at 9.4 eV.

The 396 nm pulse generating the VUV pump pulse is still present in the interaction area but we can disregard its influence in the present experiment for two reasons. First the power density in the interaction region is too low to ionize acetylene through multiphoton ionization, and second the dispersion in the LiF window introduces a significant time delay (several picoseconds) between the fundamental pulse and the third harmonic. With the LiF window, the sample is ionized only when the pump and probe pulses are properly synchronized. Note that the pump/probe signal can also be observed without the LiF window, but with a contrast of only 50% due to higher harmonics.

An additional source of information is the time-resolved ion-mass signal. The probe pulse is focused halfway between the ion and photoelectron spectrometers making the beam diameters and hence the overlap with the pump pulse the same for the two spectrometer source regions. Positive ions are collected in a 70 cm field-free time-of-flight tube and detected by an electron multiplier (EMT). The inevitable flow of xenon from the pulsed jet used for harmonic generation into the ion spectrometer is used as a cross-correlation

monitor gas: when pump and probe pulses are synchronized, xenon atoms are ionized through a nonresonant two photon-ionization process.

The photoelectron spectrometer is a truncated hemispherical electrostatic analyzer with a 144 mm radius employing a four-element retarding lens and a two-dimensional multichannel detection system. The detector consists of a matched set of microchannel plates with a phosphor screen. The analyzer may be operated in fixed lens potential mode for a given pass energy, or the potentials can be swept through the kinetic energy region of the spectrum. Each event is recorded using a video camera and the integration of the signal is made on the camera and charge-coupled device array. This multichannel electron detection allows us to effectively compensate for the relatively low spectrometer transmission. There is an aperture and a slit between the gas cell and the lens making an effective acceptance angle of less than 0.05%. A second slit at the entrance to the analyzer makes an effective vertical acceptance angle of about  $1^\circ$ . The gas sample is ionized in a continuously pumped gas cell with a pressure of approximately 0.01 mbar. The background pressure is  $3.0 \times 10^{-8}$  mbar. For this experiment the spectrometer was run at a pass energy of 20 eV resulting in a nominal energy resolution of 50 meV. For these experiments the measured spectrometer full width at half maximum (FWHM) is approximately 100 meV. The difference between the optimal resolution and the measured value arises primarily from the ion cloud which builds up with each laser pulse. The space charge effects are severe in this case.

The spectral width of the 396 nm pulses is measured to be  $2.5 \pm 0.1$  nm ( $170 \text{ cm}^{-1}$ ), which corresponds to a 90 fs Fourier-limited pulse. The temporal width of the pulse is longer than its Fourier transform limit, due to group velocity dispersion in different optical components (beam splitters, windows, crystals) affecting both the fundamental and frequency doubled pulses. In addition, the use of high energy pulses also leads to self-phase modulation in these optical components, which is much more difficult to control and estimate than group velocity dispersion.<sup>20</sup> After accounting for these effects, we estimate the pulse duration of the probe to be  $260 \pm 30$  fs, with a positive (approximately linear) chirp. The spectral width of the pump pulse can be estimated using perturbation theory to be larger by a factor of  $\sqrt{3}$  compared to the generating pulse. This produces a nominal pulse width of  $290 \text{ cm}^{-1}$  corresponding to a Fourier limited temporal duration of 50 fs. Since the laser field generating the harmonics is positively chirped, it is reasonable to expect a similar chirp of the harmonic pulse.<sup>21</sup> In addition, dispersion in the LiF window leads also to positive frequency chirp. The pulse duration and chirp of the pump (and probe) pulses are extracted from a multifit procedure where photoelectron and photoion pump-probe signals in  $\text{C}_2\text{H}_2$  and  $\text{C}_2\text{D}_2$ , as well as Xe ion cross-correlation data, are taken into account. This procedure is described in detail in Sec. IV.

The experiment was performed at two fundamental laser wavelengths producing slightly different harmonic energies:  $\lambda_1 = 132.2$  nm (9.378 eV) and  $\lambda_2 = 132.0$  nm (9.390 eV). These wavelengths were verified by comparing the photoelectron kinetic energies from the ns REMPI spectra<sup>5</sup> and the

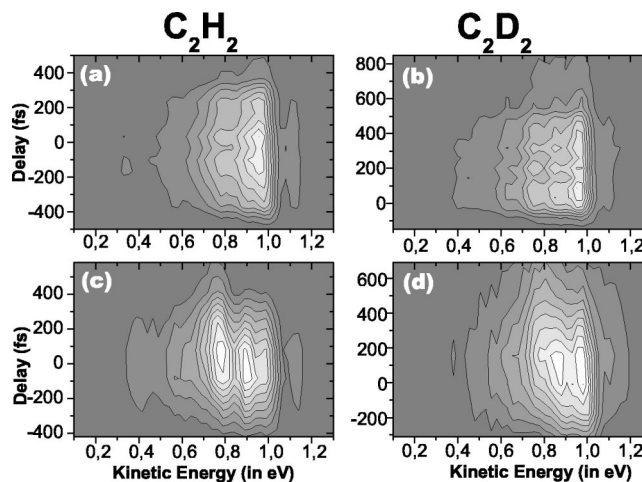


FIG. 5. In the upper part of the figure [(a) and (b)], the photoelectron spectra recorded at  $\lambda_1 = 132.2$  nm at different pump-probe delays are presented as contour plots for both isotopes. The excited bands are (a) the  $F 4_0^2$  Rydberg state in  $\text{C}_2\text{H}_2$  and (b) the  $E 5_0^2$  valence state in  $\text{C}_2\text{D}_2$ . The intensity of the entire photoelectron spectrum varies with the pump-probe delay. In the lower part, the photoelectron spectra recorded at  $\lambda_2 = 132.0$  nm (c) in  $\text{C}_2\text{H}_2$  and (d) in  $\text{C}_2\text{D}_2$ . For both isotopes, the PES contour plots show two main structures in energy with a clear difference in temporal dynamics.

ones from the present fs pump-probe experiment. Referring to the upper panel of Fig. 2 we note that for both isotopes the  $\lambda_1$  pulse initiates dynamics primarily from the  $F 4_0^2$  Rydberg state in  $\text{C}_2\text{H}_2$  (2 quanta in the *trans*-bending modes) and from the  $E 5_0^2$  valence state in  $\text{C}_2\text{D}_2$  (2 quanta in the *cis*-bending modes). The other bands involved are excited with optical intensities less than 15% of the maximum. The  $\lambda_2$  pulse, on the other hand, leads to excitation of two initial states: in  $\text{C}_2\text{H}_2$ , the  $F 4_0^2$  Rydberg and the quasi-degenerate  $E 4-5_0^2$  valence states are excited, while the  $E 5_0^2$  and  $E 4_0^2$  valence states in  $\text{C}_2\text{D}_2$ . In the case of excitation at  $\lambda_1$ , the chirp of the pump pulse would be mainly visible through the rising edge of the pump-probe signal effectively prolonging the time during which the laser frequency is resonant.<sup>22,23</sup> In the case of two excited states (at  $\lambda_2$ ), a chirp will also cause the two states to be excited at different times since the pump frequency is in resonance with the two states at different times within the pulse. The Wigner representation of the  $\lambda_2$  pump laser field is plotted in Fig. 2 (lower panel), assuming a linear frequency chirp as discussed above. Second-order dispersion  $\phi'' = +5330 \text{ fs}^2$  causes the temporal FWHM to increase from 50 to 300 fs, with the lower frequencies arriving first. The Wigner representation illustrates that this chirped pulse effectively excites the  $F 4_0^2$  Rydberg state in  $\text{C}_2\text{H}_2$  about 300 fs before the  $E$  valence state. This difference in time is not large enough to be observed in an integrated signal like the ion signal,<sup>24</sup> especially when one optical transition is weaker than the other one. Excitation of two states with different energies is visible in the final-state photoelectron kinetic energies and this makes it possible to deduce the relaxation times separately for each excited state.

### III. PHOTOELECTRON SPECTRA

In Fig. 5, contour plots of photoelectron spectra of  $\text{C}_2\text{H}_2$  and  $\text{C}_2\text{D}_2$  using a pump wavelength at  $\lambda_1 = 132.2$  nm [(a)

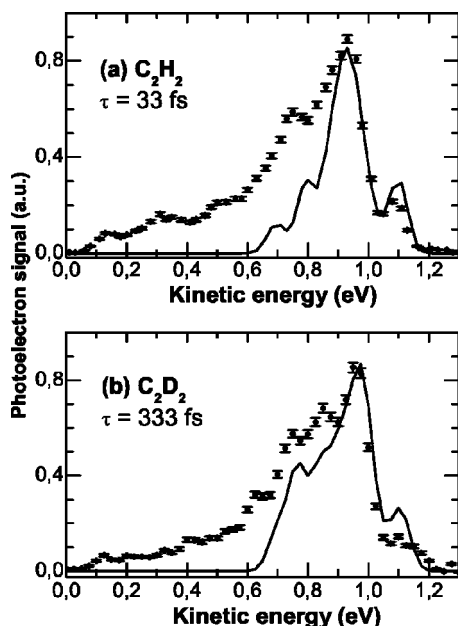


FIG. 6. For (a)  $C_2H_2$  and (b)  $C_2D_2$ , a femtosecond photoelectron spectrum (scatter plot) recorded at  $\lambda_1$  is compared to the (3+1) ns-REMPI photoelectron spectrum (solid plot) recorded at the maximum of the absorption bands in Fig. 3, corresponding to (a) a  $F 4_0^2$  Rydberg state in  $C_2H_2$  and (b) an  $E 5_0^2$  valence state in  $C_2D_2$ . The (3+1) ns-REMPI photoelectron spectra is convoluted by a 100 meV Gaussian for comparison with the fs photoelectron spectra.

and (b)] or  $\lambda_2 = 132.0$  nm [(c) and (d)], are presented as a function of the delay between the pump and probe pulses. The background spectra measured using only the 9.4 eV pump pulse and using only the 3.15 eV probe were subtracted from all photoelectron spectra. This background corresponds to only 10% of the signal maximum recorded around delay “0.”

The spectra excited with the  $\lambda_1$  pulse show essentially one photoelectron band whose amplitude varies with the time delay [Figs. 5(a) and 5(b)]. The spectra measured after excitation with  $\lambda_2$  for both isotopes are more complex [Figs. 5(c) and 5(d)]. These spectra appear to have at least two different features, which follow different temporal developments.

In Fig. 6 we present (a)  $C_2H_2$  and (b)  $C_2D_2$  PES excited at  $\lambda_1$ . We have chosen the spectra at the time delay which results in the maximum photoelectron signal and we compare them to PES recorded in (3+1) ns-REMPI plotted as a solid line.<sup>5</sup> These ns-REMPI PES have been recorded with a 30 meV total energy resolution, at resonance with (a) the maximum of the  $F 4_0^2$  Rydberg state absorption band in acetylene and (b) with the maximum of the  $E 5_0^2$  valence state in  $C_2D_2$ . The ns-REMPI spectra are broadened to the 100 meV FWHM measured on the fs-photoelectron spectrometer. We expect to see features arising from ionization of the same excited state in the fs and ns experiments, even though in the ns-REMPI spectrum, differences in measurement techniques result in narrower lines and a limited kinetic energy region since electron kinetic energies below 0.4 eV are not measured. Due to a similar geometry of the ground electronic states of neutral acetylene and its cation and to the

fact that dissociated molecules cannot be ionized, the ns-REMPI spectrum contains the main features arising from zero time-delay pump-probe ionization. Therefore many of the features in the fs spectrum can be identified. The most intense peak in the spectrum (at  $\sim 0.9$  eV) thus arises from the  $2\nu_4$  Renner–Teller multiplet of the Rydberg  $F 4_0^2$  state. In the  $C_2D_2$  spectrum the corresponding peak is assigned to the  $2\nu_5$  band of the  $E 5_0^2$  state.<sup>5</sup> For both isotopes, the weaker component at 1.1 eV is the adiabatic peak of the excited state.<sup>25</sup> At  $\lambda_1$ , the pump pulse populates mainly one initial state. Since the total energy put into the system is identical for the ns and fs experiments, it is clear that the similarities between the two photoelectron spectra reflect the Franck–Condon factors for ionization from the excited state. Their difference at higher internal energy of the parent ion (i.e., lower kinetic energy of the emitted photoelectron) is mainly the imprint of the decay through the Franck–Condon region, as well as the signature of the continuum underlying this excitation range. We find no evidence for dynamical features in the spectra shown in Figs. 5(a) and 5(b). The photoionization involved here is not sensitive to any nucleus or electronic wave-packet motion since no photoelectron dynamics is visible on the contrary to Refs. 26 and 27. The most obvious reason for this is that the total energy (9.4 + 3.14 eV) is not sufficient for accessing excited states of the acetylene ion and that the resolution is not sufficient to resolve the Renner–Teller structure of the ionic ground state.<sup>28</sup> The first rules out observation of any ionization dynamics arising from a change of the electronic interaction in the neutral molecule,<sup>29</sup> while the second prevents observation of nuclear wave-packet dynamics.

Figure 7 shows the  $C_2H_2$  PES recorded at the excitation wavelength  $\lambda_2$  at a range of pump-probe delays. The two features pointed out in Fig. 5(c) are clearly visible at 0.7 and 0.9 eV kinetic energy. We compare with the ns-REMPI spectra<sup>5</sup> for the same total energy, to identify the features. The  $F 4_0^2$  Rydberg band identified in Fig. 6 is still visible at  $-90$  fs pump-probe delay, while at 400 fs the photoelectron spectrum is mainly characterized by a  $\sim 0.7$  eV peak. This is compared to the ns-REMPI spectrum in the same way as the previous spectra and identified as ionization of the quasi-degenerate  $E 4-5_0^2$  valence state. The difference of 200 meV observed between the main component of the two photoelectron spectra, while the Franck–Condon image will lead to a difference of only 25 meV observed on the excitation spectrum, is due to the combination of the nonlinear geometry of the  $E$  valence state and the Renner–Teller effect that underlies the photoionization.<sup>5</sup> The  $\lambda_2$  excited fs spectrum is similar to the  $\lambda_1$  spectrum for the  $F$  state and to the (3+1) ns-REMPI spectrum at the energy of the  $E$  valence state. By doing such a comparison, all features in the spectrum are accounted for. The relative weights of these two features are clearly time-dependent and they decay with different lifetimes. In addition, the dynamic time-energy signature of the pulse interacting with the molecule will shift the dynamic behavior of these two features if they arise from excited states with different energies. This is because the *time-energy scale* of the pump pulse and the *time-energy benchmark* of the molecule are matched, as discussed further in Sec. IV.

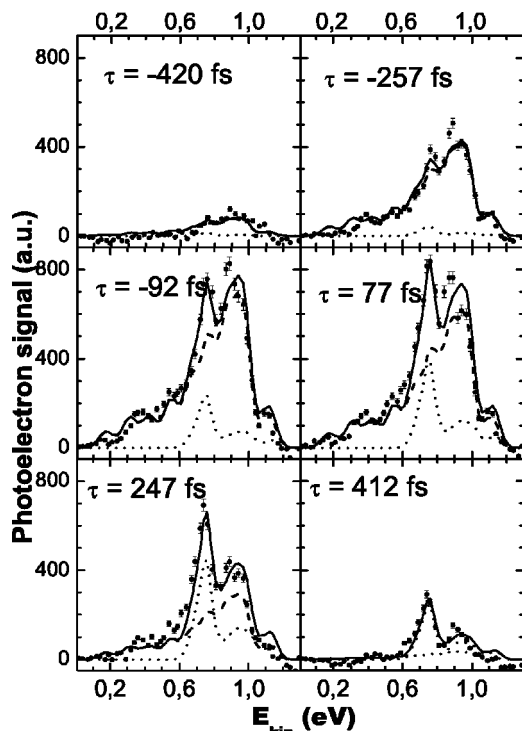


FIG. 7. Photoelectron spectra in  $C_2H_2$  recorded at  $\lambda_2=132.0$  nm (scatter plots) for a series of delay times. The dotted lines represent the PES obtained via (3+1) ns-REMPI from the  $E 4-5_0^2$  states and convoluted by a 100 meV Gaussian. The dashed lines represent the fs-PES from the  $F 4_0^2$  state recorded at  $\lambda_1$  and shown in Fig. 6(a). Their sum is plotted using a solid line in order to compare with the fs-PES.

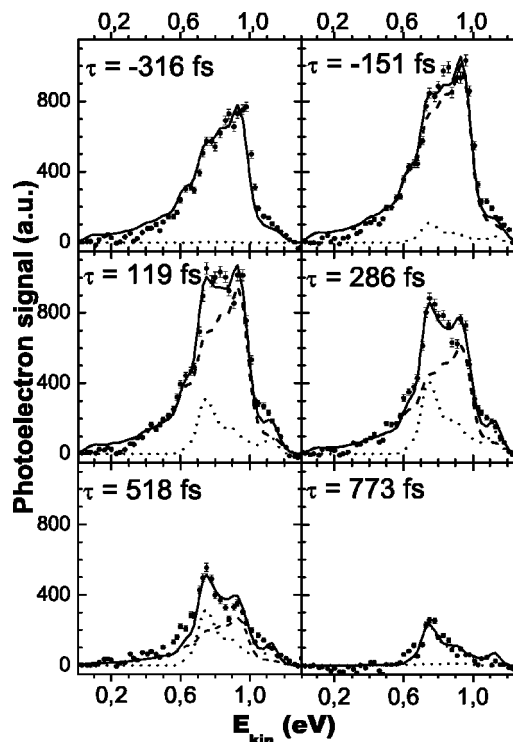


FIG. 8. Identical to Fig. 7 for  $C_2D_2$ . The dotted lines represent the PES obtained via (3+1) ns-REMPI from the  $E 4_0^2$  state. The dashed lines represent the fs-PES from the  $E 5_0^2$  state recorded at  $\lambda_1$  and shown in Fig. 6(b). Their sum is plotted using a solid line in order to compare with the fs-PES.

Figure 8 shows the time-resolved PES for  $C_2D_2$  recorded in experimental conditions identical to the  $C_2H_2$  case. Comparing the two sets of spectra we note that for short pump-probe time delays the features are similar: the lower energy level, the  $E 5_0^2$  valence state, is excited first. The decay of this state is initiated while the pulse sweeps through to the next resonant excitation, namely the  $E 4_0^2$  state. This higher-energy state dominates the photoelectron spectrum for longer pump-probe delays. The time features observed in Fig. 8 have been identified through the similarity of the fs PES and the ns-REMPI-PES for these valence states.

For both isotopes, the electronic state excited later in the pump pulse is also characterized by a set of Renner–Teller components which decay together showing no dynamical behavior. The photoelectron spectra can be simulated by using the ns-REMPI spectra as model features which simply decay on their respective time scales without including any dephasing time that would be a signature of a nucleus or electronic wave-packet motion. To summarize, from the  $\lambda_2$  analysis of Fig. 7 (Fig. 8), we distinguish in  $C_2H_2$  (in  $C_2D_2$ ) the time-dependency of the quasi-degenerate  $E 4-5_0^2$  valence state ( $E 4_0^2$  state) from the time-dependency of the Rydberg  $F 4_0^2$  state ( $E 5_0^2$  state) observed also at  $\lambda_1$ . This allows us to deduce the (time dependent) relative weight of the excitations to the different states, which will be used in the temporal analysis presented below.

## IV. TEMPORAL ANALYSIS

### A. Description of the model

Keeping the basic spectral analysis in mind, we use the information in our set of spectra to deduce the lifetimes of the excited states and the temporal characteristics of the pump and probe pulses. The time-resolved Xe ion signal provides the cross-correlation time between the pump and probe pulses directly. The temporal dynamics of photoelectron spectra and the ion-yield spectra also depend on the lifetimes of the electronic states contributing to the spectra. Since we have already determined that wave-packet dynamics can be neglected,<sup>30</sup> we can treat the system using a simplified model. A three-level system consisting of the ground state, the excited state, which decays exponentially, and a final (continuum) state is sufficient. The large spectral width of the PES averages any effect due to a chirp of the probe.<sup>31</sup> Each pump-probe signal can be written as

$$S_{\delta_s}(\Delta t) \propto \left| \int_{-\infty}^{+\infty} dt \int_0^{\infty} dt' E_p(t-t') \times e^{-i(\omega_{Lp}-\omega_e)(t-t')-i\alpha_p(t-t')^2} E_s(t-\Delta t) \times e^{-i(\omega_{Ls}-\omega_f)(t-\Delta)-i\alpha_s(t-\Delta)^2} e^{-t'/2\tau_e} \right|^2, \quad (1)$$

in which  $\tau_e$  is the decay time of the excited state with energy  $\hbar\omega_e$  above the ground state. The final state lies  $\hbar\omega_f$  above the excited state.  $E_p(t)$  and  $E_s(t)$  are the Gaussian envelopes of the pump and the probe fields, respectively, defined as

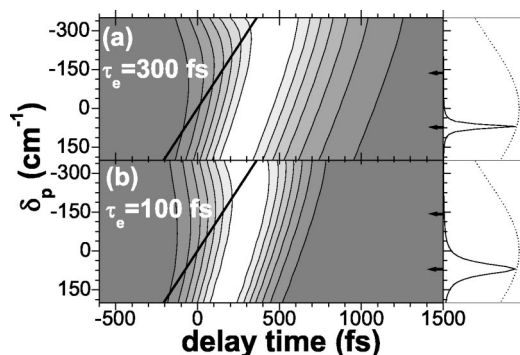


FIG. 9. Simulated pump-probe signals from a (a)  $\tau_e = 300$  fs or (b)  $\tau_e = 100$  fs excited state for different detunings of the central frequency of the exciting pulse from the resonance frequency for the electronic state,  $\delta_p$ . The contour plot follows a grayscale with the lighter shade as the maximum of pump-probe signal. The chirped pump pulse duration is 300 fs and the probe pulse is a 90 fs Fourier limited pulse for both simulations. The resonance frequencies encountered at  $\lambda_2$  in  $C_2D_2$  are indicated by the horizontal arrows. The pump frequency sweep is the solid line. The Lorentzian bandwidths of the excited states (solid plot) are shown and may be compared to the broad  $290\text{ cm}^{-1}$  pump field bandwidth (Gaussian dot plot) on the right-hand panel.

$E_i(t) = \exp[-2 \ln(2)t^2/\tau_i^2]$ .  $\tau_p$  and  $\tau_s$  are the durations of pump and probe pulses, respectively,  $\Delta t$  the pump-probe delay, while  $\tau_{0p}$  and  $\tau_{0s}$  are the Fourier limited FWHM.  $\alpha_p$  and  $\alpha_s$  are the chirp coefficients related to the quadratic dispersion  $\phi''$  as follows (with  $i = p$  or  $s$ ):

$$\alpha_i = \frac{2\phi_i''}{[\tau_{0i}^2/2 \ln(2)]^2 + 4\phi_i''^2}. \quad (2)$$

We introduce the resonant detunings  $\delta_p = \omega_{Lp} - \omega_e$  and  $\delta_s = \omega_{Ls} - \omega_f$  where  $\omega_{Lp}$  and  $\omega_{Ls}$  are the central frequencies of the pump and probe fields. Since the final state is in a continuum, the pump-probe signal is obtained by integrating  $S_{\delta_s}(\Delta t)$  over the probe spectral profile  $2\delta_f$  ( $\delta_f = 85\text{ cm}^{-1}$ ).

The total signal takes the following expression:

$$S_{\text{theo}}(\Delta t) \propto \int_{-\delta_f}^{+\delta_f} d\delta_s S_{\delta_s}(\Delta t) \alpha_e e^{-\Delta t/\tau_e} e^{(\tau_{0p}^2 + \tau_{0s}^2)/8\tau_e^2} \times \int_{-\delta_f}^{+\delta_f} d\delta_s e^{(\delta_s \alpha_s \tau_{0s}^2 \tau_s^2 - \delta_p \alpha_p \tau_{0p}^2 \tau_p^2)/2\tau_e} \times \left| 1 - \Phi \left( \frac{\gamma \sqrt{\beta_s + \beta_p}}{2\sqrt{\beta_s \beta_p}} \right) \right|^2, \quad (3)$$

where  $\gamma = (i\beta_p \delta_s - i\beta_s \delta_p - 2\beta_p \beta_s \Delta t) / (\beta_p + \beta_s) + 1/2\tau_e$  and  $\Phi$  is the error function. The coefficients  $\beta_p$  and  $\beta_s$  characterize the chirps as follows (with  $i = p$  or  $s$ ):

$$\beta_i = \frac{4 \ln 2}{\tau_i^2} + i\alpha_i. \quad (4)$$

The instantaneous frequency of the pump field,  $\omega_p(t) = \omega_{Lp} + 2\alpha_p t$ , is represented as a dashed line in the Wigner contour plots in Figs. 2(c) and 2(d). The time dependence of the pump-probe signals appears in the exponential term and in the error function in Eq. (3).

In Fig. 9, we illustrate the concept of a *time-energy*

*benchmark* by simulating the pump-probe signal of a single excited state defined by its excitation band and a varying laser wavelength (or conversely defined by a varying detuning  $\delta_p$  at a fixed laser wavelength). Several independent simulations have been carried on using Eq. (1) for different values of detuning  $\delta_p$  and are presented in a 2D contour plot (reversed grayscale), in the  $(\delta_p, \Delta t)$  plane, since the evolution of the temporal profile as a function of  $\delta_p$  is smooth and regular. The electronic state is treated as a homogeneously decaying state defined by a  $1/2\tau_e$  Lorentzian absorption band of (a)  $\tau_e = 300$  fs and (b)  $\tau_e = 100$  fs. The pump pulse is linearly chirped from 50 to 300 fs while the probe pulse is transform limited to 90 fs. On the same contour plot is drawn the instantaneous frequency  $\omega_p(t)$  (bold solid straight line in Fig. 9). To illustrate the frequency scale of the relevant quantities, we have plotted the laser profile (dotted line) and the spectral line shape (solid line) on the right-hand panel. Two tick marks correspond to the two resonances encountered at  $\lambda_2$  in  $C_2D_2$ .

Several features can be observed in Fig. 9: For a given detuning, the maximum pump-probe signal “lags” after the zero time delay. Indeed, the population increases up to the “end” of the pump pulse. This time lag is reduced when the excited state lifetime is ultrashort compared to the pump pulse duration (pump-probe signal equivalent to the cross-correlation) and for large positive detuning (and positive chirp).<sup>32</sup> This simulation can be used to understand the case of several transitions lying simultaneously within the laser bandwidth: The pump pulse excites them sequentially as the pulse frequency comes into resonance. The shift between the maxima associated to these two resonances is clearly observable. The overall pump-probe signal consists of the incoherent sum of the two contributions. Thanks to this shift, it can be easily analyzed, even when the lifetimes are of similar magnitude.

The point illustrated in Fig. 9 is that the pump pulse is defined by its *time-energy scale*: the chirp links the bandwidth and the duration of the pump pulse together. The pump-probe signal ties the *time-energy scale* of the pump and the *time-energy benchmark* of the excited state together.<sup>32</sup> Owing to the chirp imparted to the pump field, the pump-probe signal varies significantly as a function of detuning.<sup>32</sup> These are the direct result of the competition between the coherent transients defining the building-time of the population and the decay process.<sup>32</sup> This allows us in principle to fully characterize the *time-energy benchmark*, i.e., position of the resonance energy and the decay time. Conversely, for a fully characterized molecule, the behavior of the time-dependent signal should allow us to determine the central frequency and the chirp of the pump laser. In the present work, neither the chirp of the pump field nor the lifetime of the excited state are known exactly. However, we do know the resonance detuning. In addition, we have several pump-probe signals which depend directly on the chirp of the pump pulse. Note that since the final state is in the continuum, a chirp of the probe pulse does not provide a *time-energy scale*. It only decreases the time-resolution and hence attenuates the effect of the *time-energy scale* of the pump pulse.



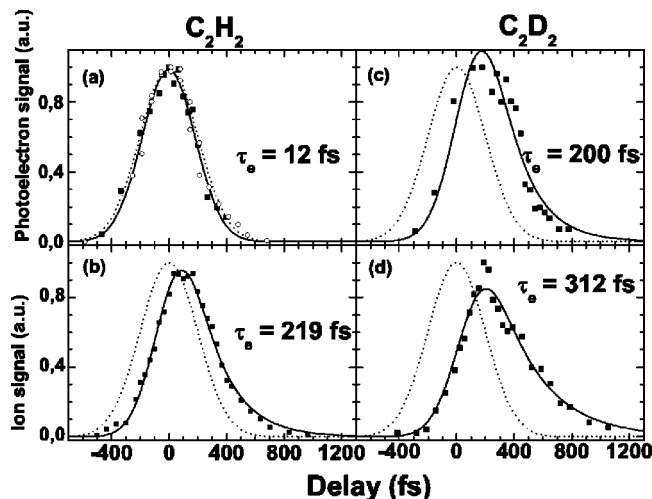


FIG. 10. Result of the multifit procedure of the PES signal [(a) :  $C_2H_2$ , (c) :  $C_2D_2$ ] and the ion [(b) :  $C_2H_2$ , (d) :  $C_2D_2$ ] as function of the pump-probe delay, for a central pump wavelength of 132.2 nm. The experimental data are plotted with closed squares. The result of the fitting procedure is plotted using a solid line. The measured and fitted cross-correlation signals on Xe are compared in (a) and the fit is reproduced in (b)–(d). The values of the parameters derived by the multifit procedure are collected in Table I.

To determine the lifetime  $\tau_e$  of each excited state as well as the chirp of the pump and probe pulses  $\alpha_p$  and  $\alpha_s$ , we perform a multifit operation. It involves a simplex optimization of the Err function defined as follows:

$$\text{Err} = \sum_n \frac{\text{Err}_n}{N_n},$$

with the index  $n$  linked to the  $n$ th pump-probe signal (such as photoion or photoelectron spectrum, for  $C_2H_2$  and  $C_2D_2$ ),  $N_n$  is the number of data points in the pump-probe signal, and  $\text{Err}_n$  is the error to minimize for each delay. The input parameters are the Fourier limited duration of the VUV pump and probe pulses as well as the resonance detuning  $\delta_p$  between the pump carrier frequency and the maximum of the absorption band for each of the excited states.

## B. Results and discussion at $\lambda_1$

Figure 10 shows the experimental data at  $\lambda_1$  (closed squares for the  $C_2H_2$  and  $C_2D_2$  data, and open circles for Xe) together with the fits (solid and dotted lines) obtained from the multifit procedure described above. Note that the time-dependency of the photoelectron is the one observed in Figs. 5(a) and 5(b). The top curves show (a) the acetylene and (c) deuterated acetylene total electron signal and (a) the Xe ion signal. The bottom curves present (b) the acetylene and (d) deuterated acetylene ion signal with the Xe fit only. The fits are in reasonable agreement with the time-resolved signals. The chirp of the pump pulse results in a pulse lengthening from 50 to 320 fs. We find a significant chirp of the probe pulse resulting in a pulse lengthening from 90 to 340 fs, slightly longer than the 260 fs estimation. This leads to a cross-correlation time of 470 fs obtained from the  $Xe^+$  signal. The results from the multifit procedure are displayed in Table I.

TABLE I. Decay times and pulse durations for the fits in Figs. 10 and 11.

at $\lambda_1 = 132.2$ nm—one excited state				
Isotope	Species	Lifetime (fs)	Excited state	Ref. 6
$C_2H_2$	ions	$219 \pm 30$	$F 4_0^2$	140 fs
	electrons	$12 \pm 6$		
$C_2D_2$	ions	$312 \pm 30$	$E 5_0^2$	
	electrons	$200 \pm 20$		
Pump duration (fs)		$326 \pm 30$		
Probe duration (fs)		$340 \pm 30$		
at $\lambda_2 = 132.0$ nm—two excited states				
Isotope	Species	Lifetime (fs)	Excited state	Refs. 6 and 3
$C_2H_2$	ions	$171 \pm 25$	quasi degenerate	143 fs
	electrons	$147 \pm 15$	$E 4 - 5_0^2$	
$C_2D_2$	ions	$600 \pm 20$	$E 4_0^2$	210 fs
	electrons	$644 \pm 45$		
Pump duration (fs)		$280 \pm 30$		
Probe duration (fs)		$340 \pm 30$		

The similarity between the cross-correlation and the electron signal in Fig. 10(a) clearly indicates that the temporal resolution is not sufficient to determine the decay time of the excited state. The time dependence of the  $C_2H_2^+$  ion signal [Fig. 10(b)], however, is significantly slower than that measured in the PES. We attribute this difference to a more selective decay channel for the measured electron spectra. The photoelectron spectrometer lens makes the transmission highly directionally selective. The detected electrons are emitted in a narrow cone (less than  $1^\circ$ ) in the horizontal plane, while the ion time-of-flight spectrometer has nearly  $4\pi$  transmission. The transition to the  $F^1\Sigma_u^+$  Rydberg state is a  $\Sigma^+ - \Sigma^+$  transition, preferentially selecting acetylene molecules with the CC axis parallel to the polarization of the pump field. The entrance axis of the photoelectron spectrometer is perpendicular to both pump and probe polarizations. We propose two explanations for the striking difference between the ion and electron signals. One possibility assumes a resonant pump-probe excitation scheme where no photoelectron emission takes place in the horizontal plane whatever the transient state encountered during the dynamics. Then the time-dependence observed in the PES would follow the cross-correlation signature resulting from nonresonant excitation and would be identical to the Xe cross correlation spectrum. However, for all time delays the PES shown in Fig. 5 clearly exhibits the signature of the  $F 4_0^2$  state in the  $2\nu_4$  Renner–Teller multiplet.

A second explanation involves two dissociation processes, where one is monitored in the electron spectrum. A fast dissociation process producing electrons emitted predominantly in the horizontal plane and visible with an angular selective photoelectron detector, and a slower process emitting electrons mainly in other planes would explain this discrepancy. The  $4\pi$  detection ion signal contains the two dissociation channels, however, the slower one is the dominant channel. This has similarly been observed by recording photofragment action spectra of the  $C_2H$  radicals for a

$^1\Pi_u(3d\delta_g)$  Rydberg state lying  $\sim 6000\text{ cm}^{-1}$  above the  $F$  state.<sup>6,33</sup> These spectra indicate two open dissociation channels: (i) a very fast dissociation (femtosecond time scale) in a quasi-linear geometry leading to fast H fragments and to  $\text{C}_2\text{H}(A^2\Pi)$  fragments with low vibrational excitation in the stretching modes; and (ii) a slower dissociation (picosecond time scale) taking place in nonlinear geometry and leading to slow H fragments and  $\text{C}_2\text{H}(A^2\Pi)$  fragments with a broad, structureless statistic-like energy and isotropic angular distributions.<sup>6,33</sup> This broad internal energy distribution in the  $\text{C}_2\text{H}(A^2\Pi)$  fragments corresponds to highly excited bending levels, as was recently shown by the analysis of the  $\text{C}_2\text{H}$  fragment emission spectra,<sup>11</sup> and is compatible with a slow dissociation process leaving time to the nuclei for large amplitude bending motion.

For the  $F$  Rydberg state and  $E$  state, the photofragment action spectra of Ref. 6 were recorded after excitation to the vibrational  $2_0^1$  and  $4-5_0^2$  levels, respectively, leading to similar conclusions.<sup>6</sup> The angular emission patterns for the states measured in this study might provide conclusive information about this matter. A study of the photoelectron spectra from these states using an imaging detector would be an advantage,<sup>34</sup> as recently achieved in other femtosecond time-resolved experiments on photodissociation dynamics<sup>35</sup> and intersystem crossing.<sup>36</sup> Relevant information to understand the difference between the ion and the photoelectron decay might also be obtained by comparing the angular dependence of ns-PES and fs-PES. In reality, even for dissociation which is fast compared to the rotational period of the parent molecule, we would expect that the predissociation occurs with a significant change of geometry.<sup>35</sup> This would lead to dynamics visible in the electron kinetic energies and intensities, and in the angular dependence of electron emission. Clearly our experiment would benefit by having a higher photon energy in the probe pulse where fragment states could be ionized.

We can compare our value of 200 fs with the 140 fs lifetime estimate from the spectral linewidth of  $\text{D}^+$  photofragmentation from the  $E\ 5_0^2$  valence state in  $\text{C}_2\text{D}_2$  (see Table I). The photofragment action spectra of the  $\text{C}_2\text{D}$  radical does not show an angular dependency as strong as the ones observed in  $\text{C}_2\text{H}$ , while still exhibiting two dissociation channels.<sup>6</sup> This is in line with the similarity that we observe between the decay times observed for the ion and angle-selected photoelectron signal.

### C. Results and discussion of $\lambda_2$

The discussion regarding the excitation of two states with the same pulse makes it clear that the analysis of the spectra will be more complex than for the first excitation wavelength. The analysis is done on seven different sets of pump-probe signals: the two temporal components in the electron spectra and the ion yield for both isotopes, the xenon cross-correlation data. The time-dependencies of these spectra are presented in Fig. 10. The fit is carried out in the same way as earlier; the fixed input parameters are the Fourier limited pulse durations, the resonance detunings, and the decay behaviors found at  $\lambda_1$  excitation for the  $F$  Rydberg state for the electron (earliest temporal component) and ion

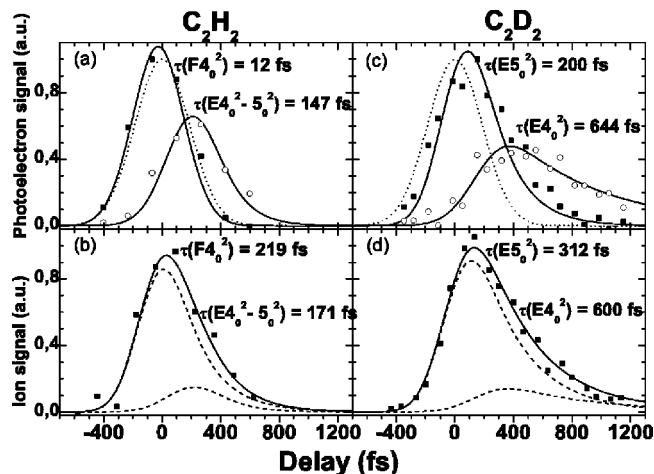


FIG. 11. Result of the fit of the PES signal as a function of the pump-probe delay for a central pump wavelength of 132.0 nm in (a)  $\text{C}_2\text{H}_2$  and (c)  $\text{C}_2\text{D}_2$ . The ion-yield spectra measured simultaneously are shown in (b) and (d). The time development of the two PES components are shown separately in each frame together with the results of the fit (solid lines). The cross-correlation fit obtained from the Xe signal is plotted in dotted lines in (a) and (c).

signals in  $\text{C}_2\text{H}_2$  and similarly the decay at  $\lambda_1$  for the  $E\ 5_0^2$  valence state in  $\text{C}_2\text{D}_2$ . The lifetimes  $\tau_e$  of the quasi-degenerate  $E\ 4-5_0^2$  valence state for  $\text{C}_2\text{H}_2$  and the  $E\ 4_0^2$  valence state for  $\text{C}_2\text{D}_2$  and the chirp of the pulses  $\alpha_p$  and  $\alpha_s$  are then deduced through the multifit procedure.

The fitted values for these parameters are displayed in Table I. The lifetimes of the electronic states deduced from the width of the action photodissociation peaks<sup>6</sup> are included in the table for comparison. It is worth noting that lifetimes evaluated in Ref. 6 always have to be taken as lower limits, since it is assumed that observed bandwidths exclusively originate from predissociation broadening. This point has been discussed in Ref. 11 (Fig. 3) where, for instance, the apparent very short lifetime of the  $H$  Rydberg state actually results from two broad overlapping transitions and, therefore, has to be corrected by first deconvoluting these overlapping bands.

We expect the chirp to be about the same for both wavelengths, which is confirmed by the fitted value of 280 fs for the pump and 340 fs for the probe pulse. The fact that the chirp on the visible light pulse deduced from the multiparameter fits is identical for the two wavelengths studied speaks in favor of our analysis method. Figure 11 shows the fits including separate contributions from each state. The good agreement between the fits and the PES time dependence again confirms the validity of the multifit procedure. The more complex fit is a more stringent test of the model since two time-energy benchmarks with a known decay time and detuning are used to describe the  $F\ 4_0^2$  in  $\text{C}_2\text{H}_2$  and the  $E\ 5_0^2$  state in  $\text{C}_2\text{D}_2$ .

Looking at the plots in Fig. 11 we see that before 200 fs in  $\text{C}_2\text{H}_2$  and 300 fs in  $\text{C}_2\text{D}_2$  the features discussed at  $\lambda_1$  dominate. This is expected since the pump frequency sweep will reach the state of lower absorption energy first. The relative weights of the components should be determined by the pulse energy distribution and by the oscillator strength

for the transition as well as by their respective detunings. In  $C_2H_2$  the stronger feature corresponds to the  $F$  state relative to the  $E$  state confirming the weight ratio obtained by integrating the absorption bands of the two states over the broad pump bandwidth. In addition, for the same decay time, a positive detuning will lead to a slightly stronger pump-probe signal than a negative detuning, and this effect increases with the chirp of the pump pulse.<sup>32</sup> This behavior is stronger in the ion signal than in the photoelectron signal, possibly due to a strong angular dependence of the photoelectron emission from the  $F$  state compared to the  $E$  state. In  $C_2H_2$ , the  $E$  valence state lifetime is significantly longer than the Rydberg state lifetime, confirming the results deduced from spectroscopy on  $H$  photofragments.<sup>2,3,22</sup> In the  $C_2D_2$  spectra the intensity distribution of the exciting pulse accounts for the intensities of the two features. An interesting result is the significant difference in the decay times observed in  $C_2D_2$ : the excitation of the *cis* mode seems to lead to a faster predissociation dynamics than the excitation of the *trans* mode. This tendency is also observed in the  $H$  photofragment spectrum.<sup>6</sup> Finally, the ion signal can be reproduced from an incoherent sum of the two pump-probe signals. In agreement with that already observed at  $\lambda_1$  in  $C_2D_2$ , the decay time deduced from the ion signal is of the same order of magnitude as the PES decay time. No strong angular dependence of the PES is expected.

## V. CONCLUSIONS

Ultrashort VUV pulses allow photoinduced dynamics for higher valence-excited states in molecules to be studied. However, in this excitation range, the electronic state density is significant making any meaningful temporal analysis difficult. In order to distinguish the electronic states excited by a pump pulse which overlaps two or more levels, we have combined a PES analysis with a linear chirp of the pump frequency. The pump chirp supplies a *time-energy scale* such that each electronic excited state can be identified in the PES. We illustrate this method on the predissociation of  $F$  and  $E$  states in  $C_2H_2$  and  $C_2D_2$ .

The simultaneous analysis of the time-dependent electron and ion-yield spectra together with the Xe cross-correlation data reveals the time-dependent evolution of each electronic state. In acetylene we find lifetimes between about 20 and 200 fs, in d-acetylene these lifetimes are somewhat longer, ranging up to about 600 fs. The difference between the electron and ion-yield time dependencies is interpreted by the angle selectivity of our electron spectrometer, which detects only those electrons emitted with a given symmetry.

A VUV femtosecond pulse would also be useful as a probe, to directly photoionize the atomic photofragments, so that the electron kinetic energies and angular distributions could be recorded or to reach the excited states of ion. In that case, nonadiabatic coupling via a photoionization pump-probe experiment might be elucidated by photoionization dynamics in the excited states of the ion.<sup>37</sup> In many small polyatomic molecules, a VUV femtosecond probe pulse would be particularly useful for this kind of application.

- <sup>1</sup>M. P. Bernstein, J. P. Dworkin, S. A. Sandford, G. W. Cooper, and L. J. Allamandola, *Nature (London)* **416**, 401 (2002); G. M. Munoz Caro, U. J. Meierhenrich, W. A. Schutte, B. Barbier, A. A. Segovia, H. Rosenbauer, W. H.-P. Thiemann, A. Brack, and J. M. Greenberg, *ibid.* **416**, 403 (2002).
- <sup>2</sup>P. Löffler, D. Lacombe, A. Ross, E. Wrede, L. Schnieder, and K. H. Welge, *Chem. Phys. Lett.* **252**, 304 (1996).
- <sup>3</sup>M. Kono, K. Hoshina, and K. Yamanouchi, *J. Chem. Phys.* **117**, 1040 (2002).
- <sup>4</sup>M. Herman and R. Colin, *J. Mol. Spectrosc.* **85**, 449 (1981).
- <sup>5</sup>V. Blanchet, S. Boyé, S. Zamith, A. Campos, B. Girard, J. Lievin, and D. Gauyacq, *J. Chem. Phys.* **119**, 3751 (2003), preceding paper.
- <sup>6</sup>P. Löffler, E. Wrede, L. Schnieder, J. B. Halpern, W. M. Jackson, and K. H. Welge, *J. Chem. Phys.* **109**, 5231 (1998).
- <sup>7</sup>K. Resch, V. Blanchet, A. Stolow, and T. Seidemann, *J. Phys. Chem. A* **105**, 2756 (2001).
- <sup>8</sup>A. Assion, T. Baumert, M. Geisler, V. Seyfried, and G. Gerber, *Eur. Phys. J. D* **4**, 145 (1998).
- <sup>9</sup>J. A. Davies, J. E. LeClaire, R. E. Continetti, and C. C. Hayden, *J. Chem. Phys.* **111**, 1 (1999); V. Stert, H.-H. Ritze, E. T. J. Nibbering, and W. Radloff, *Chem. Phys.* **272**, 99 (2001); S. Lochbrunner, T. Schultz, M. Schmitt, J. P. Shaffer, M. Z. Zgierski, and A. Stolow, *J. Chem. Phys.* **114**, 2519 (2001).
- <sup>10</sup>A. Campos, S. Boye, P. Brechignac, S. Douin, C. Fellows, N. Shafizadeh, and D. Gauyacq, *Chem. Phys. Lett.* **314**, 91 (1999).
- <sup>11</sup>Y.-C. Hsu, F.-T. Chen, L.-C. Chou, and Y.-J. Shiu, *J. Chem. Phys.* **105**, 9153 (1996).
- <sup>12</sup>A. Lauter, K. S. Lee, K. H. Jung, R. K. Vatsa, J. P. Mittal, and H.-R. Volpp, *Chem. Phys. Lett.* **358**, 314 (2002).
- <sup>13</sup>S. Boyé, A. Campos, S. Douin, C. Fellows, D. Gauyacq, N. Shafizadeh, P. Halvick, and M. Boggio-Pasqua, *J. Chem. Phys.* **116**, 8843 (2002).
- <sup>14</sup>F. Seifert, J. Ringling, F. Noack, V. Petrov, and O. Kittelmann, *Opt. Lett.* **19**, 1538 (1994); A. L'Huillier and P. Balcou, *Phys. Rev. Lett.* **70**, 774 (1993).
- <sup>15</sup>L. Nugent-Glandorf, M. Scheer, D. A. Samuels, A. M. Mulhisen, E. R. Grant, X. Yang, V. M. Bierbaum, and S. R. Leone, *Phys. Rev. Lett.* **87**, 193002 (2001).
- <sup>16</sup>M. Bauer, C. Lei, K. Read, R. Tobey, J. Gland, M. M. Murnane, and H. C. Kapteyn, *Phys. Rev. Lett.* **87**, 025501 (2001); L. Misoguti, S. Backus, C. G. Durfee, R. Bartels, M. M. Murnane, and H. C. Kapteyn, *ibid.* **87**, 013601 (2001).
- <sup>17</sup>A. Nazarkin, G. Korn, O. Kittelmann, J. Ringling, and I. V. Hertel, *Phys. Rev. A* **56**, 671 (1997); M. Wittmann, M. T. Wick, O. Steinkellner, P. Farmanara, V. Stert, W. Radloff, G. Korn, and I. V. Hertel, *Opt. Commun.* **173**, 323 (2000).
- <sup>18</sup>S. L. Sorensen, O. Björneholm, I. Hjelte *et al.*, *J. Chem. Phys.* **112**, 8038 (2000).
- <sup>19</sup>R. Bartels, S. Backus, E. Zeek, L. Misoguti, G. Vdovin, I. P. Christov, M. M. Murnane, and C. Kapteyn, *Nature (London)* **406**, 164 (2000).
- <sup>20</sup>G. P. Agrawal, *Nonlinear Fiber Optics* (Harcourt, New York, 1989).
- <sup>21</sup>J. Norin, J. Mauritsson, A. Johansson *et al.*, *Phys. Rev. Lett.* **88**, 193901 (2002); T. K. T. Sekikawa, S. Miura, and S. Watanabe, *ibid.* **88**, 193902 (2002).
- <sup>22</sup>S. Zamith, J. Degert, S. Stock, B. De Beauvoir, V. Blanchet, M. A. Bouchene, and B. Girard, *Phys. Rev. Lett.* **87**, 033001 (2001).
- <sup>23</sup>S. Zamith, Thèse d'université, Paul Sabatier, 2001.
- <sup>24</sup>V. Blanchet, M. Zgierski, Z. C. Yan, T. Seidemann, S. Lochbrunner, J. J. Larsen, M. Schmitt, J. P. Shaffer, and A. Stolow, *Faraday Discuss. Chem. Soc.* **115**, 33 (2000).
- <sup>25</sup>N. Shafizadeh, J. H. Fillion, D. Gauyacq, and S. Couris, *Philos. Trans. R. Soc. London, Ser. B* **355**, 1637 (1997).
- <sup>26</sup>A. Assion, M. Geisler, J. Helbing, V. Seyfried, and T. Baumert, *Phys. Rev. A* **54**, R4605 (1996); C. Meier and V. Engel, *Chem. Phys. Lett.* **212**, 691 (1993).
- <sup>27</sup>M.-C. Heitz, G. Durand, F. Spiegelman, and C. Meier, *J. Chem. Phys.* **118**, 1282 (2003); S. Vajda, C. Lupulescu, A. Merli, F. Budzyn, L. Wöste, M. Hartmann, J. Pittner, and V. Bonai-Koutecký, *Phys. Rev. Lett.* **89**, 213404 (2002).
- <sup>28</sup>J. E. Reutt, L. S. Wang, J. E. Pollard, D. J. Trevor, Y. T. Lee, and D. A. Shirley, *J. Chem. Phys.* **84**, 3022 (1986); S. T. Pratt, P. M. Dehmer, and J. L. Dehmer, *ibid.* **99**, 6233 (1993); M. Peric and J. Radic-Peric, *Chem. Phys. Lett.* **290**, 443 (1998).
- <sup>29</sup>V. Blanchet, M. Z. Zgierski, and A. Stolow, *J. Chem. Phys.* **113**, 1194 (2001).

- <sup>30</sup>M. Seel and W. Domcke, *J. Chem. Phys.* **95**, 7806 (1991).
- <sup>31</sup>S. Meyer, C. Meier, and V. Engel, *J. Chem. Phys.* **108**, 7631 (1998).
- <sup>32</sup>S. Zamith, J. Degert, S. Stock, B. de Beauvoir, V. Blanchet, M. A. Bouchène, and B. Girard, in *Femtochemistry and Femtobiology: Ultrafast Dynamics in Molecular Science*, edited by A. Douhal and J. Santamaria (World Scientific, Singapore, 2002), p. 559.
- <sup>33</sup>J.-H. Wang, Y.-T. Hsu, and K. Liu, *J. Phys. Chem. A* **101**, 6593 (1997).
- <sup>34</sup>A. T. J. B. Eppink and D. H. Parker, *Rev. Sci. Instrum.* **68**, 3477 (1997); M. J. J. Vrakking, *ibid.* **72**, 4084 (2001).
- <sup>35</sup>J. A. Davies, R. E. Continetti, D. W. Chandler, and C. C. Hayden, *Phys. Rev. Lett.* **84**, 5983 (2000).
- <sup>36</sup>M. Tsubouchi, B. J. Whitaker, L. Wang, H. Kohguchi, and T. Suzuki, *Phys. Rev. Lett.* **86**, 4500 (2001).
- <sup>37</sup>V. Blanchet, M. Z. Zgierski, T. Seidemann, and A. Stolow, *Nature (London)* **401**, 52 (1999).